

Overexpression of interleukin-4 using adeno-associated virus is a potential strategy to enhance bone regeneration

Hyewon Kim¹ , Kyong-Hwa Kim², Leewoo Kang¹, Yang-Jo Seol², Shin Hye Chung^{3,*},
Shin-Young Park^{1,*}

¹Department of Dental Science, Dental Research Institute, School of Dentistry, Seoul National University, Seoul 03080, Republic of Korea

²Department of Periodontology, Dental Research Institute, School of Dentistry, Seoul National University, Seoul 03080, Republic of Korea

³Department of Dental Biomaterials Science, School of Dentistry and Dental Research Institute, Seoul National University, Seoul 03080, Republic of Korea

*Corresponding authors: Shin-Young Park, Program of Clinical Dental Education and Dental Research Institute, School of Dentistry, Seoul National University, 101 Daehak-ro, Jongno-gu, Seoul 03080, Republic of Korea (nalby99@snu.ac.kr) and Shin Hye Chung, Department of Dental Biomaterials Science, Dental Research Institute, School of Dentistry, Seoul National University, 101 Daehak-ro, Jongno-gu, Seoul 03080, Republic of Korea (den533@snu.ac.kr)

Abstract

This study aimed to investigate the bone regeneration potential of IL-4 gene delivery via adeno-associated virus (AAV) vectors, with a particular focus on modulating macrophage polarization and promoting osteogenic differentiation. Four different AAV serotypes (AAV1, AAV2, AAV5, and AAV6) encoding the IL-4 gene were evaluated in rat and human gingival fibroblasts and dental pulp stem cells (DPSCs). AAV2 exhibited the highest transduction efficiency and IL-4 expression in all tested cell types. IL-4 transduced DPSCs demonstrated enhanced osteogenic differentiation, as evidenced by the upregulation of osteogenic markers, increased alkaline phosphatase activity, and elevated calcium deposition. IL-4 transduction activated the extracellular signal-regulated kinase signaling pathway, contributing to osteogenesis. To assess the therapeutic efficacy of AAV2-IL-4 in vivo, a lipopolysaccharide-induced calvarial osteolysis model was established in C57BL/6 mice. AAV2-IL-4 administration significantly reduced bone resorption, as confirmed by micro-CT and histological analysis. Moreover, IL-4 gene delivery promoted M2 macrophage polarization. These findings highlight AAV2-IL-4 as a promising gene therapy strategy for bone regeneration, effectively integrating immunomodulation and osteogenesis to counteract inflammation-driven bone loss.

Keywords: interleukin-4, gene therapy, adeno-associated virus, dental pulp stem cell, bone regeneration

Lay Summary

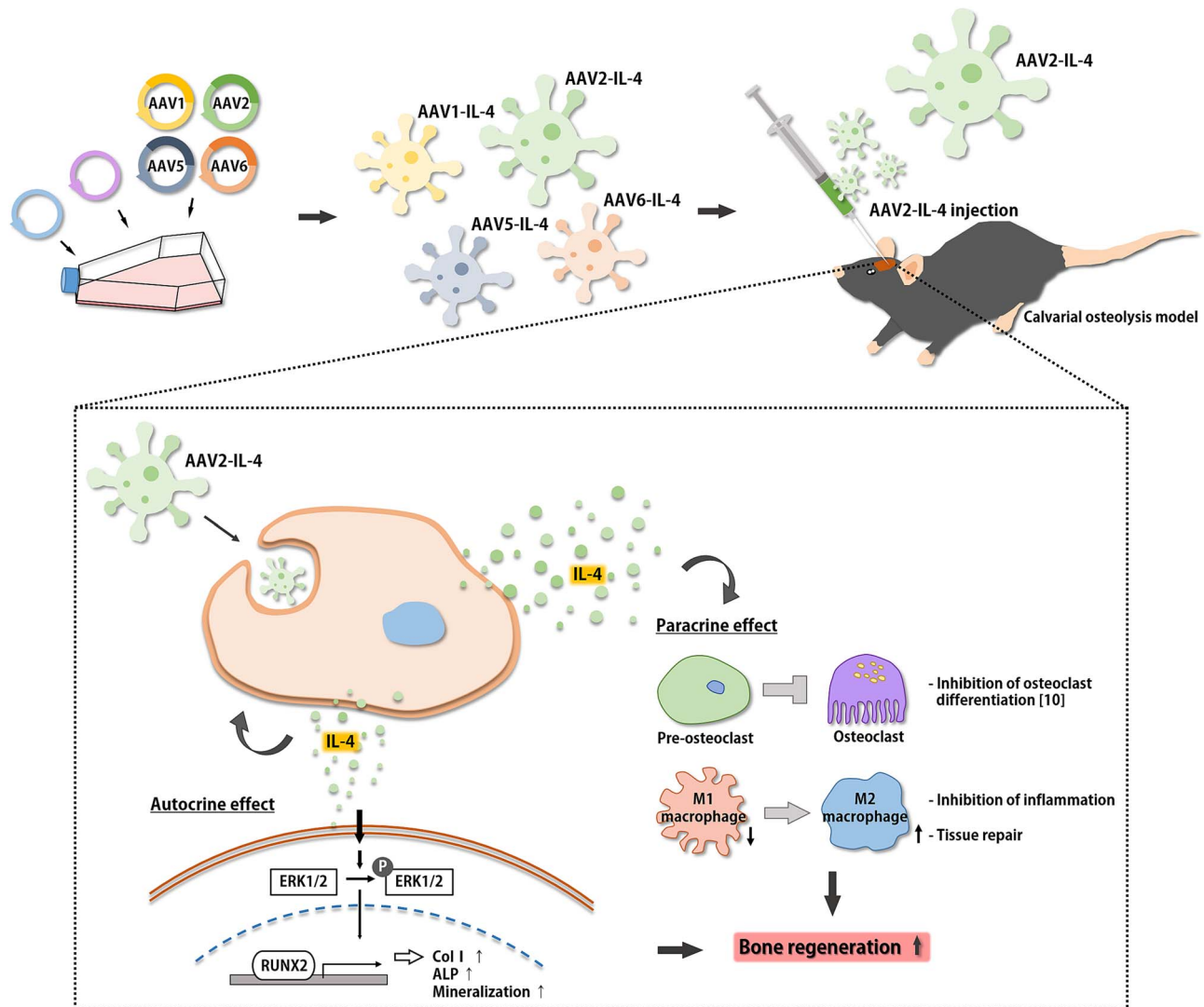
Bone loss due to inflammation is a major concern. This study explored a gene therapy using an adeno-associated virus (AAV) to deliver the IL-4 gene, an anti-inflammatory molecule that regulates immune responses and supports bone healing. Among 4 AAV types tested, AAV2 most effectively delivered IL-4 into two types of dental-related cells: gingival fibroblasts and dental pulp stem cells. In a mouse model of inflammation-induced bone loss, AAV2-IL-4 reduced bone destruction by promoting M2 macrophage polarization and enhancing bone formation. These findings suggest AAV2-IL-4 could be a promising strategy for immune modulation and bone regeneration in inflammatory bone diseases.

Received: December 9, 2024. Revised: March 20, 2025. Accepted: April 2, 2025

© The Author(s) 2025. Published by Oxford University Press on behalf of the American Society for Bone and Mineral Research.

This is an Open Access article distributed under the terms of the Creative Commons Attribution Non-Commercial License (<https://creativecommons.org/licenses/by-nc/4.0/>), which permits non-commercial re-use, distribution, and reproduction in any medium, provided the original work is properly cited. For commercial re-use, please contact journals.permissions@oup.com

Graphical Abstract



Introduction

Periodontal disease is characterized by inflammation-induced bone destruction resulting from bacterial infection; however, this bone loss is not solely attributed to the accumulation of pathogenic bacteria.¹ Instead, environmental factors and host-specific immune responses are closely related to disease progression.² In particular, the host's susceptibility to bacterial invasion and the severity of the inflammatory response are critical determinants of alveolar bone destruction.³

Macrophages, derived from monocytes, are key regulators of the interaction between the immune system and bone metabolism.⁴ In response to specific stimuli, macrophages can polarize into 2 distinct phenotypes: pro-inflammatory M1 or anti-inflammatory M2 macrophages. M1 macrophages, activated by interferon-gamma (IFN- γ) and lipopolysaccharide (LPS), produce pro-inflammatory cytokines such as tumor necrosis factor-alpha (TNF- α), interleukin-1 (IL-1), and IL-6.⁵ These cytokines enhance osteoclast activity, leading to increased bone resorption.⁶ In chronic inflammatory conditions such as rheumatoid arthritis and periodontal disease, macrophages contribute to the imbalance in

bone homeostasis by promoting inflammation and bone loss.⁷

Conversely, macrophages can also exert anti-inflammatory effects through M2 polarization. Activated by IL-4 or IL-13, M2 macrophages secrete anti-inflammatory cytokines such as transforming growth factor-beta (TGF- β), IL-4, IL-10, and IL-13, which support tissue repair and bone formation.⁸ Among these cytokines, IL-4 plays a pivotal role in bone healing by counteracting pro-inflammatory signals, mitigating inflammation, and creating a regenerative microenvironment conducive to bone repair.⁹ Additionally, IL-4 enhances M2 macrophage polarization and osteogenesis, exhibiting greater efficacy than IL-10 and IL-13 in promoting both immunomodulation and bone formation.¹⁰ In addition to its immunomodulatory properties, IL-4 has been implicated in bone repair through its upregulation during fracture healing, inhibition of bone resorption, and preservation of essential bone characteristics, such as trabecular bone volume and local bone geometry.^{11,12}

Tissue regeneration in damaged sites typically occurs 2-3 wk after the initial inflammatory phase.¹³ To support this

process, researchers have developed various strategies for the sustained release of regenerative biomaterials. In this context, gene delivery systems, particularly adeno-associated virus (AAV) vectors, can be considered to maximize the osteogenic effects of IL-4.¹⁴ By enabling *in vivo* production of IL-4, AAV-mediated gene delivery sustains IL-4 expression, modulating the local inflammatory response through autocrine and paracrine signaling. Unlike protein delivery at a concentration of 0.5–1.0 mg/mL in a single administration, AAV-based gene delivery maintained target molecules for up to 2 wk at concentrations ranging from 200 to 6000 pg/mL.¹⁵ This prolonged release pattern mimics physiological bone regeneration processes, with prior studies demonstrating enhanced bone maturation without the lace-like woven bone associated with high-dose BMP administration.¹⁶ However, the osteogenic potential of AAV-mediated IL-4 gene delivery has not been fully investigated.

This study aims to investigate the osteogenic differentiation potential of IL-4 gene delivery in dental pulp stem cells (DPSCs) using 4 AAV serotypes (AAV1, AAV2, AAV5, and AAV6) and to assess their transduction efficiency. Given that periodontitis leads to the destruction of alveolar bone, the goal of this study is to explore a regenerative strategy that specifically targets periodontal bone loss. DPSCs were selected as the primary cell model due to their high proliferative capacity, multilineage differentiation potential, and significant regenerative capability in bone tissue engineering, particularly in periodontal bone regeneration.¹⁷ The *in vitro* experiments determine the ability of IL-4 to promote osteogenic differentiation in DPSCs, providing insights into potential therapeutic strategies for bone regeneration. To validate these findings, the study also evaluates the impact of IL-4 gene delivery on bone regeneration *in vivo* using a LPS-induced calvarial osteolysis model in C57BL/6 mice. The osteolytic calvarial defect model represents the pathophysiological conditions of bone resorption observed in human diseases such as osteoporosis and periodontitis. By evaluating the role of IL-4 in regulating osteogenic differentiation and macrophage polarization, this study aims to provide valuable insights into the therapeutic potential of IL-4 gene delivery for bone regeneration, particularly in the treatment of inflammatory bone loss.

Materials and methods

Cell culture

Rat gingival fibroblasts (rGFs), human dental pulp stem cells (hDPSCs), and human gingival fibroblasts (hGFs) were purchased from Cell Biologics, LONZA, and ScienCell, respectively. All experiments were conducted using cells within 5 passages from the original vials. Rat dental pulp stem cells (rDPSCs) were isolated from 10-wk-old Sprague-Dawley rats obtained from Orient Bio and characterized. All procedures were approved by the Institutional Animal Care and Use Committee of Seoul National University (SNU-210510-1-2). The rDPSC primary culture was performed following a previously established protocol.¹⁸ Briefly, after euthanasia via carbon dioxide inhalation, the lower jaws were separated and divided into two hemi-jaws. A small hole was made at the apical foramen for pulp tissue extraction; then, the pulp tissue was fragmented and digested with 1.5 mg/mL of collagenase I (Thermo Fisher Scientific) for 40 min at 37 °C. The isolated cells were then grown in Minimum Essential Medium

Eagle- α modification (Welgene) supplemented with 10% fetal bovine serum (Welgene) and 1% antibiotic-antimycotic solution (Welgene), and incubated in a 37 °C incubator with 5% CO₂. To identify rDPSCs, fluorescence-activated cell sorting (FACS) analysis was performed.¹⁹ Cells were incubated with antibodies against CD29-fluorescein isothiocyanate (FITC), CD90-FITC, and CD45-allophycocyanin (Thermo Fisher Scientific). FACS was conducted using the LSR Fortessa X-20 system (BD Biosciences).

AAV vector production

The pAAV-CMV vector, pRC1 vector, pRC2 vector, pRC5 vector, pRC6 vector, pAAV-ZsGreen1 vector, and pHelper vector were purchased from Takara Bio. The human IL-4 gene was cloned into the pAAV-CMV vector, producing pAAV-CMV-hIL-4 (Cosmo Genetech). HEK293 cells were used for transfection. A total of 4×10^6 cells were seeded the day before transfection. Cells were transfected with 13 μ g of pAAV-CMV-IL-4, pAAV-ZsGreen1, pRC1, pRC2, pRC5, pRC6, and pHelper vector. Two days post-transfection, cells were harvested, and viral particles were purified using the AAVpro Purification Kit (Takara Bio). Viral titers were measured by qPCR using the AAVpro Titration Kit (Takara Bio). All viral serotypes were stored at –80 °C and thawed one to three times before use.

AAV vector transduction

Rat dental pulp stem cells, rGFs, hDPSCs, and hGFs were seeded in 24-well plates at a density of 2×10^4 cells per well. Cells were transduced with the AAV vector encoding IL-4 or ZsGreen1 at a multiplicity of infection (MOI) of 1000. Following a 6-hr incubation, the transduction medium was exchanged with fresh growth medium.

Cell proliferation assay

Cell proliferation assays were performed using the Premix WST-1 Cell Proliferation Assay System (Takara Bio). rDPSCs, rGFs, hDPSCs, and hGFs were plated in 96-well plates at a density of 2×10^3 cells per well. The cells were infected with AAV1-, AAV2-, AAV5-, or AAV6-IL-4 and cultured for 3 d, with daily measurements. WST-1 solution was added to each well, followed by incubation at 37 °C for 30 min. Absorbance was measured at 450 nm using an Emax Plus Microplate Reader (Molecular Devices).

Immunofluorescence

Adeno-associated virus transduction efficiency was evaluated with fluorescence staining. rDPSCs, rGFs, hDPSCs, and hGFs were infected with AAV-ZsGreen1 at a MOI of 1000. At 72 hr post-transduction, the cells were fixed with 4% paraformaldehyde (PFA) for 10 min, washed with phosphate-buffered saline (PBS), and mounted using ProLong Diamond antifade mountant containing 4',6-diamidino-2-phenylindole (Thermo Fisher Scientific). ZsGreen1 expression was observed and captured using a confocal microscope (LSM 700; Carl Zeiss).

Enzyme-linked immunosorbent assay (ELISA)

Human dental pulp stem cells, hGFs, rDPSCs, and rGFs were infected with AAV1-, AAV2-, AAV5-, and AAV6-IL-4. Culture media were collected on days 1, 3, and 7. The IL-4 concentration in the collected media was measured using the Human IL-4 TMB ELISA Development Kit (PeproTech) according to the manufacturer's instructions.

Table 1. Primer sequence.

Gene	Forward primer (5'-3')	Reverse primer (5'-3')
Human		
IL-4	CTTTGCTGCCTCCAAGAACACA	CGAGTGTCCCTTCTCATGGTGG
Runx2	TGGTTACTGTCATGGCGGGTA	TCTCAGATCGTTGAACCTTGCT
Col1	GTGCTAAAGGTGCCAATGGT	ACCAGGTTACCCTGTTAC
Alp	ACTGGTACTCAGACAACGAGAT	ACGTC AATGTCCCTGATGTTATG
Osx	CCTCTGCGGGACTCAACAAC	AGCCCATTAGTGCTTGTA AAGG
Ocn	GGCGCTACCTGTATCAATGG	GTGGTCAGCCAACTCGTCA
Gapdh	ACATGTTCCAATATGATTCC	TGGACTCCACGACGTACTCA
Rat		
Runx2	CATGGCCGGGAATGATGAG	TGTGAAGACCGTTATGGTCAAAGTG
Col1	TCCTGCCGATGTCGCTATC	CAAGTTCGGGTGTGACTCGTG
Alp	CACGTTGACTGTGGTACTGCTGA	CCTGTAAACCAGGCCCGTTG
Osx	ATGGCGTCTCTCTGCTTG	TGAAAGGTCAGCGTATGGCTT
Ocn	CTGACCTCACAGATCCCAAGC	TGGTCTGATAGCTCGTACAAG
Gapdh	TCTCTGCTCCTCCTGTTCTA	ATGAAGGGGTGCTTGATGGC

Abbreviations: IL-4, interleukin-4; Runx2, runt-related transcription factor 2; Col1, type I collagen; Alp, alkaline phosphatase; Osx, osterix; Ocn, osteocalcin; Gapdh, glyceraldehyde-3-phosphate dehydrogenase.

Real-time PCR

Total RNA was extracted from cells using the TaKaRa MiniBEST Universal RNA Extraction Kit (Takara Bio) in accordance with the manufacturer's protocol. Complementary DNA (cDNA) was synthesized using the PrimeScript II first strand cDNA Synthesis Kit (Takara Bio) according to the manufacturer's instructions. Real-time PCR was performed using SYBR Premix Taq II (Takara Bio) and a StepOnePlus Real-Time PCR system (Applied Biosystems). The primers used are listed in Table 1. The PCR reaction was performed for 30 s at 95 °C, followed by 40 amplification cycles of 5 s at 95 °C and 30 s at 60 °C. The comparative Ct method was used to measure the level of expression. Glyceraldehyde 3-phosphate dehydrogenase (GAPDH) was used as a housekeeping gene for normalization.

Western blot analysis

Total protein was extracted using cell lysis buffer (Thermo Fisher Scientific) supplemented with a protease inhibitor (GenDEPOT) and a phosphatase inhibitor (GenDEPOT). The lysates were separated by sodium dodecyl sulfate-polyacrylamide gel electrophoresis and transferred to polyvinylidene fluoride membranes. The membranes were incubated overnight at 4 °C with primary antibodies against runt-related transcription factor 2 (Runx2) (Cell Signaling Technology), alkaline phosphatase (ALP) (Bioss Antibodies), extracellular signal-regulated kinase (ERK) (Cell Signaling Technology), phospho-ERK (Cell Signaling Technology), c-Jun N-terminal kinase (JNK) (Cell Signaling Technology), phospho-JNK (Cell Signaling Technology), p38 (Cell Signaling Technology), phospho-p38 (Cell Signaling Technology), and GAPDH (FineTest). GAPDH was used as a loading control for normalization. Protein bands were quantified using ImageJ software (U.S. National Institutes of Health).

ALP activity

Alkaline phosphatase staining was performed using the StemAb Alkaline Phosphatase Staining Kit II (Reprocell). After 7 d of osteogenic induction, the differentiated cells were fixed with fixation solution for 2 min, washed twice with PBS, and incubated with the ALP staining solution for 30 min at room temperature. Stained monolayers were visualized using an inverted microscope (Carl Zeiss).

Alizarin red S (ARS) staining and quantification

Calcium deposition was evaluated by ARS staining. After osteogenic differentiation for 21 d, the cells were fixed with 4% PFA and stained with Alizarin Red solution (Sigma-Aldrich) for 30 min. To quantify the staining, the stained cells were incubated with 10% (v/w) cetylpyridinium chloride for 10 min, and the absorbance was measured using a microplate reader at 570 nm.

LPS-induced calvarial osteolysis model and AAV2-IL-4 injection

Animal experiments were approved by the Institutional Animal Care and Use Committee of Seoul National University (IACUC, number SNU-240325-3). The LPS-induced calvarial osteolysis model was established as previously described.²⁰ Briefly, 8-wk-old male C57BL/6 mice were purchased from Orient Bio. The animals were housed in groups of up to five in filter-top cages under a 12-hr light-dark cycle at room temperature with ad libitum access to food and water. They were bred and maintained in a pathogen-free environment. *Escherichia coli* LPS (Sigma-Aldrich) was dissolved in endotoxin-free water at a concentration of 1 mg/mL. LPS (25 mg/kg) or saline was subcutaneously injected over the calvaria. The mice were monitored the following day, and no significant adverse effects were observed. Seven days after LPS injection, calvarial bone lysis was analyzed using in vivo micro-CT (Quantum GX; Revvity). After that, saline, 1×10^{11} particles of empty AAV2, or AAV2-IL-4 were injected, respectively. The animals were randomly assigned to 4 groups ($n=6$ in each group): group 1, mice injected with saline and saline; group 2, mice injected with LPS and saline; group 3, mice injected with LPS and empty AAV2; group 4, mice injected with LPS and AAV2-IL-4. Seven days after the final injection, all mice were sacrificed, and calvarial bones were fixed in 10% neutral buffered formalin for micro-CT and histological analysis.

Micro-CT imaging

Micro-CT imaging was acquired using a SkyScan 1173 (Bruker, Aartselaar, Belgium) after attaching the samples to the jig with parafilm. Scanning parameters were set to 90 kV and 88 μ A with a 1.0 mm aluminum filter, resulting in the acquisition of 800 images. The obtained images were reconstructed using NRecon software (Bruker). Following reconstruction, bone volume fraction (BV/TV),

trabecular number (Tb.N.), trabecular separation (Tb.Sp.), and trabecular thickness (Tb.Th.) were calculated using CTAn software (Bruker). The region of interest (ROI) was defined as a 3 mm diameter circular area around the midline suture of the mouse calvaria.

H&E staining

Fixed calvarial bone tissues were decalcified with 10% EDTA and dehydrated through a series of graded ethanol, and embedded in paraffin. Each calvarial tissue sample was cut into 3 μm sections using a Leica RM2255 fully automated rotary microtome (Leica Microsystems GmbH). Following sectioning, H&E staining was performed, and the stained sections were observed under an Olympus BX51 microscope (Olympus Optical Co.). Images were captured using a digital slide scanner (PANNORAMIC 250 Flash III; 3DHISTECH Ltd.).

Immunohistochemistry

Three- μm -thick sections were deparaffinized and rehydrated. The sections were treated with 3% hydrogen peroxide for 10 min. Antigen retrieval was performed by heating the sections in citrate buffer at 97 $^{\circ}\text{C}$ for 10 min. The sections were then blocked with 1% BSA and incubated at 37 $^{\circ}\text{C}$ for 1 hr with the following primary antibodies: anti-ARG1 (NBP1-32731, Novus Biologicals), anti-iNOS (NB300-605, Novus Biologicals), and anti-NF- κB (8242S, Cell Signaling Technology). The slides were incubated at room temperature for 1 hr with HRP-conjugated secondary antibodies. The slides were observed under an Olympus BX51 microscope and images were captured using PANNORAMIC 250 Flash III digital slide scanner (3DHISTECH Ltd.).

Statistical analysis

Results are presented as mean \pm SD values. One-way and two-way analysis of variance with Tukey post hoc test were performed to confirm statistical significance with the GraphPad Prism version 5.0 software (GraphPad Software). A p -value of $<.05$ was considered to indicate statistical significance.

Results

Characterization of rDPSCs

To characterize the properties of primary cultured rDPSCs, FACS analysis was performed. The cells were positive for mesenchymal stem cell (MSC) surface markers CD29 and CD90 and negative for the hematopoietic cell surface marker CD45 (Figure S1A). Multi-lineage differentiation potential was examined using oil-red o staining for lipid droplets, alizarin red staining for mineralized nodules, and alcian blue staining for acidic polysaccharides. Differentiation-induced rDPSCs exhibited positive staining for all markers (Figure S1B).

Transduction efficiency of rGFs, hGFs, rDPSCs, and hDPSCs with 4 different serotypes of AAVs using ZsGreen1

To examine the transduction efficiency of different AAV serotypes, a pAAV-ZsGreen1 vector was packaged with serotypes 1, 2, 5, and 6. rGFs, hGFs, rDPSCs, and hDPSCs were infected with AAV1, AAV2, AAV5, and AAV6 carrying the ZsGreen1 gene. Three days post-infection, ZsGreen1 fluorescence was captured and quantified. The expression of ZsGreen1 was highest in rDPSCs, and AAV2 exhibited the high transduction efficiency across all cell types (Figure 1A and B).

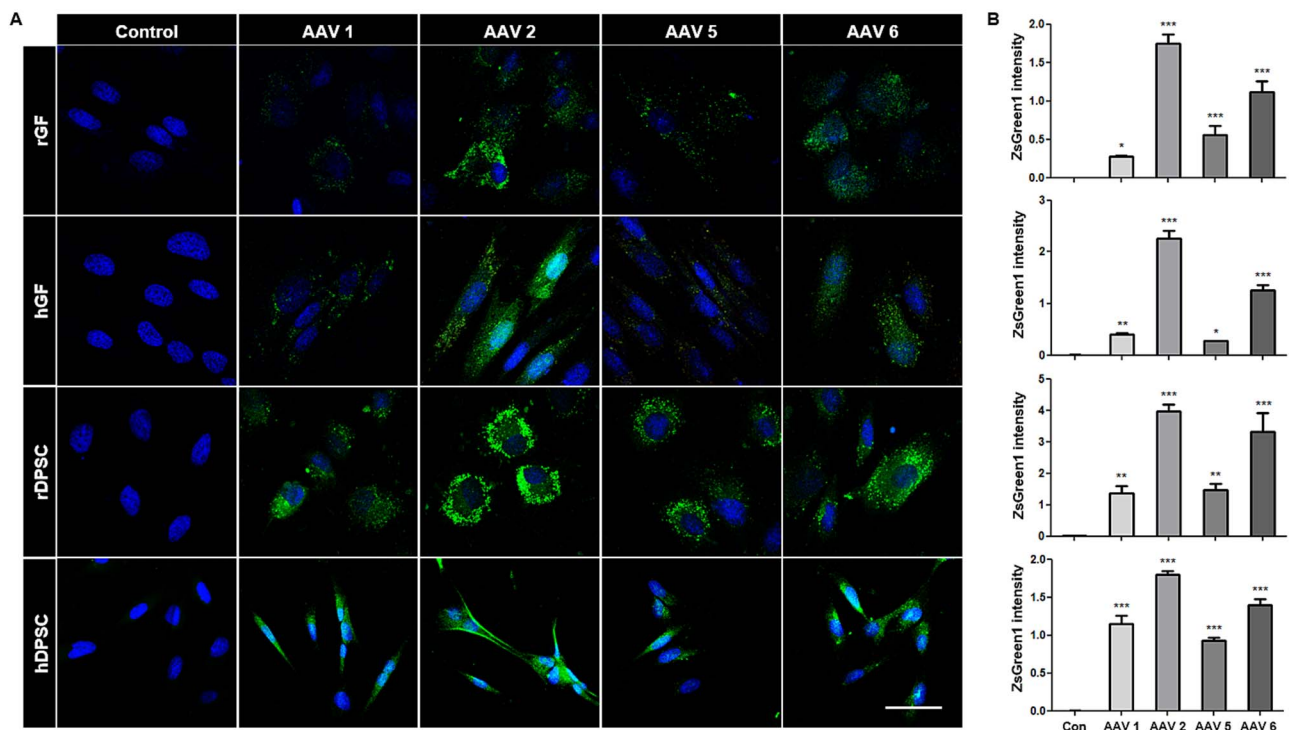


Figure 1. Comparison of AAV-ZsGreen1 expression levels on rGFs, hGFs, rDPSCs, and hDPSCs. (A) Representative confocal microscopy images of ZsGreen1 expression 3 d after AAV1-, AAV2-, AAV5-, and AAV6-ZsGreen1 transduction in rGFs, hGFs, rDPSCs, and hDPSCs. Scale bar = 50 μm . * $p < .05$. ** $p < .01$. *** $p < .001$. $N = 3$. Abbreviations: AAV, adeno-associated virus; rGFs, rat gingival fibroblasts; hGFs, human gingival fibroblasts; rDPSCs, rat dental pulp stem cells; hDPSCs, human dental pulp stem cells.

Titration and optimization of working concentration of AAV serotypes encoding IL-4

The titers of AAV1-, AAV2-, AAV5-, and AAV6-IL-4 were determined by qPCR. Among the serotypes, AAV2-IL-4 showed the highest production yield, followed by AAV1-, AAV6-, and AAV5-IL-4 (Figure 2A). To determine the optimal concentration of AAV particles for infection, cells were treated with various MOIs (10, 100, 1000, and 10000 vg/cell) for all serotypes. As shown in Figure 2B, cell viability was significantly reduced at an MOI of 10000 vg/cell, indicating cytotoxicity at this concentration. Based on these findings, an MOI of 1000 vg/cell was selected for subsequent experiments.

IL-4 expression in AAV1-, AAV2-, AAV5-, and AAV6-IL-4-transduced rGFs, hGFs, rDPSCs, and hDPSCs

The expression of IL-4 in transduced cells was quantified by qPCR 3 d post-transduction and by ELISA at various time points over a 14 d period. The introduced IL-4 gene was expressed in all cell types, with higher expression observed in human cells compared to rat cells (Figure 2C). Among the AAV serotypes, AAV2-mediated IL-4 expression was the highest, whereas AAV5-mediated expression was the lowest across all cell types (Figure 2C). Secreted IL-4 levels were similar in both human and rat cells, but were higher in human cells for up to 7 d (Figure 2D). In rGFs transduced with AAV2

and AAV6, the expression of secreted IL-4 was significantly elevated compared to the control group for 7 d (Figure 2D). The expression of secreted IL-4 introduced by AAV2, AAV5, and AAV6 was also significantly higher than that in the control group among hGFs for 7 d (Figure 2D). Although IL-4 secretion declined over time, secreted IL-4 levels in rDPSCs and hDPSCs remained significantly higher than in the control group at day 14 (Figure 2D).

Transduction of AAV1-, AAV2-, AAV5-, and AAV6-IL-4 induced osteogenic differentiation of rDPSCs and hDPSCs

To evaluate the potential of AAV1-, AAV2-, AAV5-, and AAV6-IL-4 in promoting osteogenic differentiation, the gene and protein expression levels of the osteogenic markers, as well as calcium deposition, were measured. Col1, Runx2, Alp, Osx, and Ocn messenger RNA (mRNA) levels of rDPSCs and hDPSCs were significantly higher in the AAV2- and AAV6-IL-4 groups compared to the control group (Figure 3A and B). Protein levels of RUNX2 and ALP were also significantly elevated in osteogenically differentiated rDPSCs (Figure 3C and D) and hDPSCs (Figure 3E and F) transduced with AAV1-, AAV2-, and AAV6-IL-4. Furthermore, ALP staining intensity was greater in the AAV2- and AAV6-IL-4 groups compared to the control group (Figure 3G). Consistently, calcium deposition was significantly increased

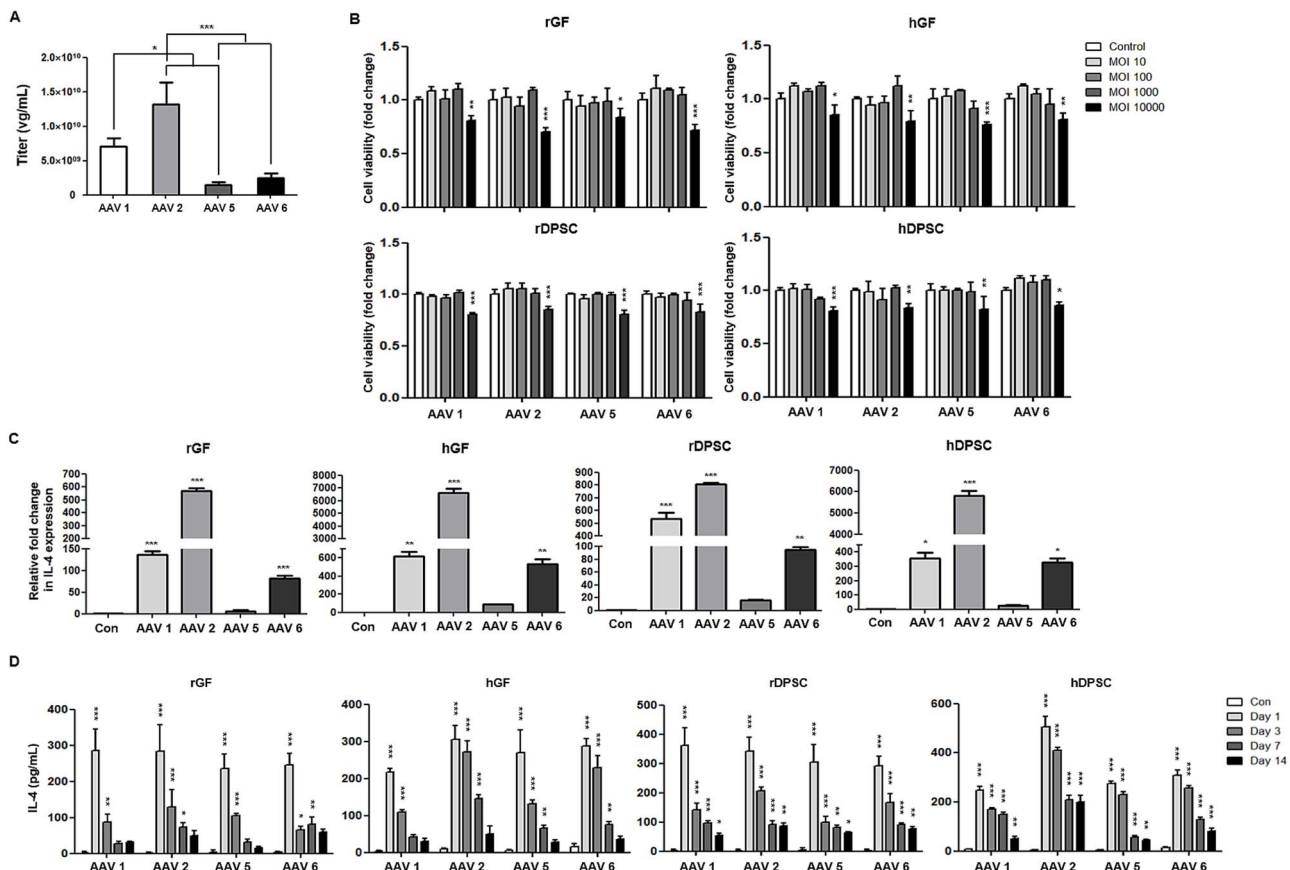


Figure 2. Comparison of titer, viability, and transduction efficiency of AAV1-, AAV2-, AAV5-, and AAV6-IL-4. (A) Titer of AAV1-, AAV2-, AAV5-, and AAV6-IL-4. (B) Viability of rGFs, hGFs, rDPSCs, and hDPSCs transduced with AAV1-, AAV2-, AAV5-, and AAV6-IL-4 at various concentrations. (C) mRNA expression of IL-4 in the rGFs, hGFs, rDPSCs, and hDPSCs at day 3 post-transduction with AAV serotypes. (D) Comparison of IL-4 protein expression levels in rGFs, hGFs, rDPSCs, and hDPSCs for 14 d post-transduction of AAV serotypes. * $p < .05$. ** $p < .01$. *** $p < .001$. $N = 3$. Abbreviations: AAV, adeno-associated virus; rGFs, rat gingival fibroblasts; hGFs, human gingival fibroblasts; rDPSCs, rat dental pulp stem cells; hDPSCs, human dental pulp stem cells.

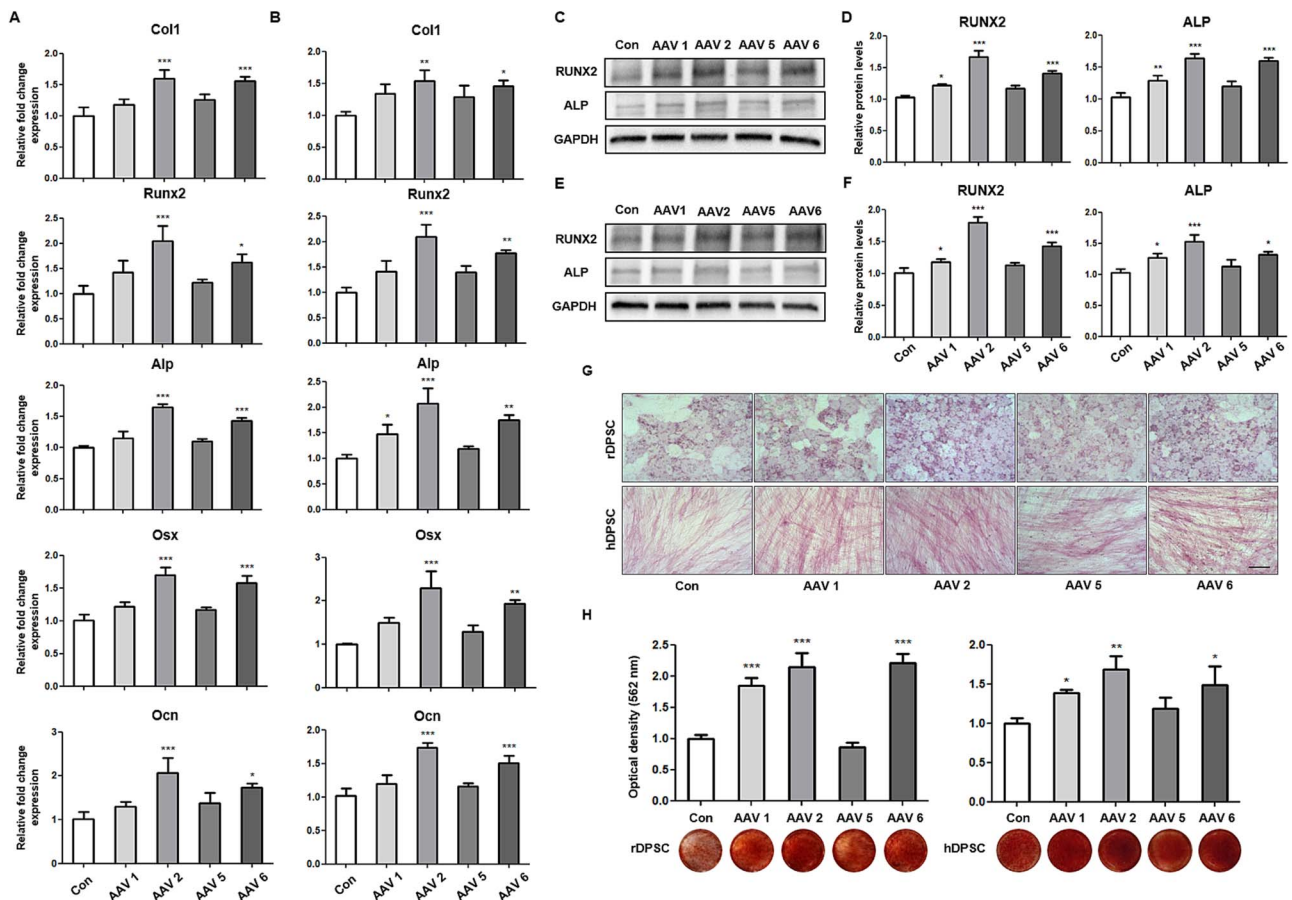


Figure 3. AAV-mediated IL4 delivery in rat and human DPSCs increased osteogenic differentiation. Osteogenic-differentiation marker gene expression (Col1, Runx2, alp, Osx, and Ocn) of rDPSCs (A) and hDPSCs (B). The expression of osteogenic-differentiation protein markers (RUNX2 and ALP) of rDPSCs (C) and hDPSCs (E) infected with AAV1-, AAV2-, AAV5-, and AAV6-IL4. (D) Quantitative analysis of intensity in (C). (F) Quantitative analysis of intensity in (E). (G) Bright-field micrographs showing ALP staining of IL4-transgenic rat and human DPSCs. (H) Calcium deposition of IL4-overexpressing rDPSCs and hDPSCs by ARS staining. GAPDH was used for normalization. Scale bar = 100 μ m. * p < .05. ** p < .01. *** p < .001. N = 3. Abbreviations: DPSCs, dental pulp stem cells; rDPSCs, rat dental pulp stem cells; hDPSCs, human dental pulp stem cells; ALP, alkaline phosphatase; GAPDH, glyceraldehyde 3-phosphate dehydrogenase; ARS, alizarin red S.

in the AAV1-, AAV2-, and AAV6-IL-4 groups relative to the control group (Figure 3H).

IL-4-transduction activated ERK signaling pathway in osteogenic differentiation

To investigate the signaling pathway associated with osteogenic differentiation induced by AAV-IL-4-transduction, the mitogen-activated protein kinase (MAPK) signaling pathway was examined by Western blotting (Figure 4A and C). No significant differences were observed in the expression levels of ERK, p-JNK, JNK, p-p38, or p38 among the groups. However, the ratio of p-ERK/ERK was significantly increased in osteogenically differentiated rDPSCs (Figure 4B) and hDPSCs (Figure 4D) transduced with AAV1-, AAV2-, AAV5-, and AAV6-IL-4.

AAV2-IL-4 injection suppressed bone damage in calvarial osteolysis model

Adeno-associated virus 2, which exhibited the highest efficacy in promoting osteogenic differentiation in vitro, was applied in vivo using a mouse calvarial osteolysis model to evaluate its bone regeneration potential. The experimental scheme is summarized in Figure 5A. In brief, bone loss was induced by subcutaneous injection of LPS around the calvaria. Seven days

after LPS injection, bone resorption was detected (Figure 5B), and saline, empty AAV2, or AAV2-IL-4 was subsequently administered. After an additional 7 d, calvaria were excised for histological analysis and micro-CT imaging.

Micro-CT results showed that AAV2-IL-4 injection reduced LPS-induced bone resorption (Figure 5C). The BV/TV ratio in the LPS + AAV2-IL-4 group was significantly higher than that in the LPS + saline or LPS + Empty AAV2 groups (Figure 5D). The Tb.N. in LPS-treated groups was significantly reduced compared to the saline-treated group (Figure 5D). The Tb.Sp. in the LPS + AAV2-IL-4 group was significantly decreased compared to the LPS + saline or LPS + Empty AAV2 groups, reaching levels comparable to those of the saline + saline group (Figure 5D).

Hematoxylin and eosin staining confirmed the protective effect of AAV2-IL-4 against LPS-induced bone erosion (Figure 5E). Bone resorption was more apparent in the LPS-treated group compared to the saline-treated group (Figure 5E, yellow dotted line). However, LPS-induced bone resorption pit regions were markedly reduced in the LPS + AAV2-IL-4 group compared to the LPS + saline or LPS + Empty AAV2 groups (Figure 5E, yellow asterisk). Additionally, Cathepsin K staining, a key enzyme in bone matrix degradation and a direct indicator of

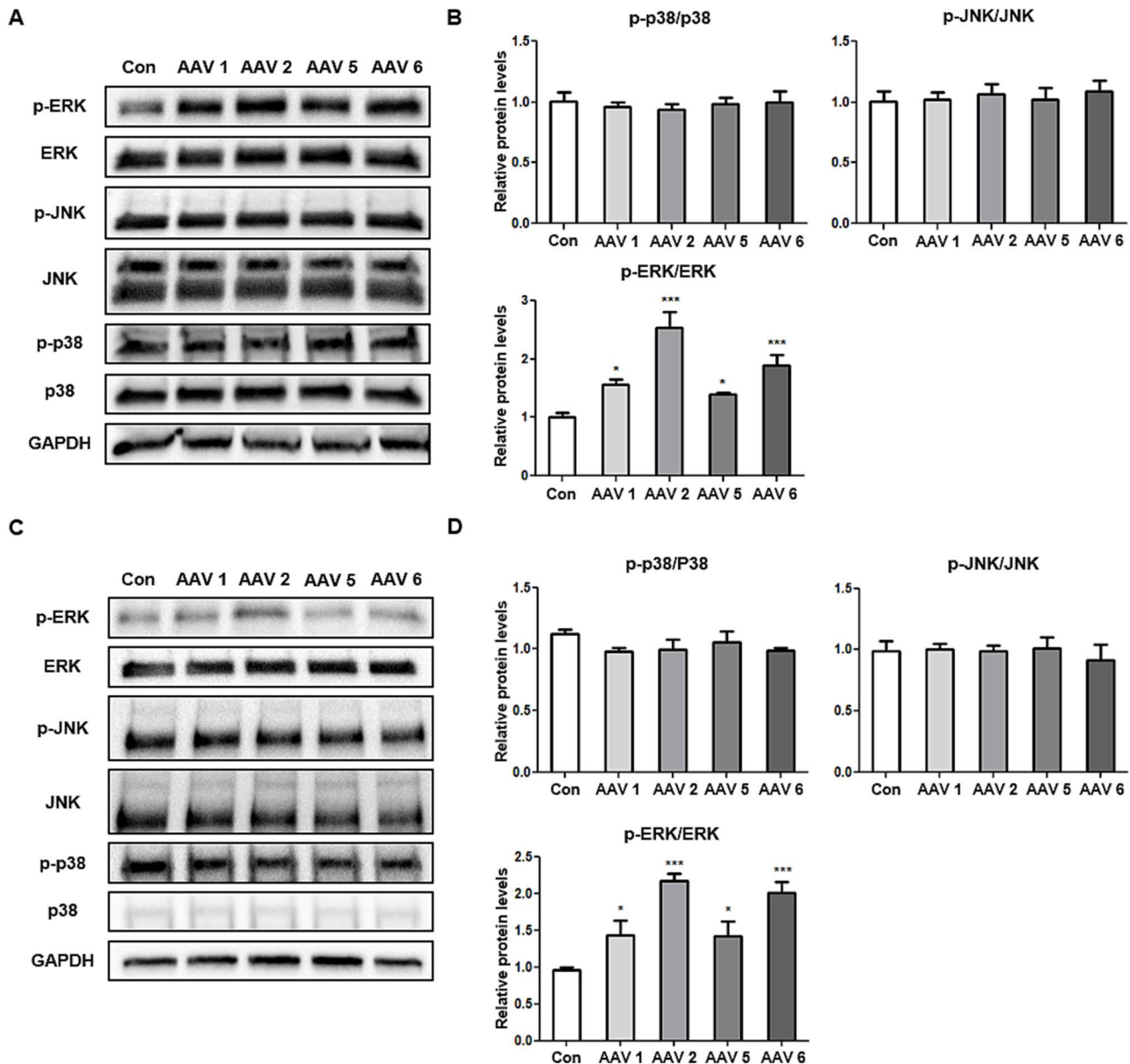


Figure 4. Signaling pathway of osteogenic differentiation related to IL-4-transgenic rat and human DPSCs. Western blot analysis of MAPK (ERK, JNK, and p38) signaling pathway proteins in IL-4-overexpressing rDPSCs (A) and hDPSCs (C). Quantitative analysis of band intensity is shown in (B) and (D). GAPDH was used for normalization. * $p < .05$. *** $p < .001$. $N = 3$. Abbreviations: DPSCs, dental pulp stem cells; MAPK, mitogen-activated protein kinase; ERK, extracellular signal-regulated kinase; JNK, c-Jun N-terminal kinase; rDPSCs, rat dental pulp stem cells; hDPSCs, human dental pulp stem cells.

osteoclast-mediated resorptive activity, was performed to identify the presence of multinucleated osteoclasts and bone resorption on bone surfaces. Cathepsin K expression on bone surfaces was increased in response to LPS treatment but was reduced in the AAV2-IL-4-treated group (Figure 5F, red arrow).

AAV2-IL-4 injection induces polarization toward M2 macrophages

Immunohistochemical analysis of calvarial sections is presented in Figure 6A. The expression of ARG1 and CD206 (M2 macrophage markers) was significantly increased in the AAV2-IL-4-treated group, whereas the expression of iNOS and CCR7 (M1 macrophage markers) was decreased (Figure 6B). No significant difference in NF- κ B expression was observed between the 2 groups.

Discussion

In the present study, we evaluated the transduction efficiency of 4 different AAV serotypes in DPSCs and GFs and demonstrated that AAV-mediated IL-4 gene delivery promotes the osteogenic differentiation of DPSCs. Additionally, the injection of AAV2-IL-4 in an LPS-induced calvarial osteolysis model exhibited a regenerative effect on damaged bone.

DPSCs and GFs play distinct but crucial roles in dental tissue regeneration.²¹ DPSCs, derived from the highly vascularized dental pulp, possess multipotency and the ability to differentiate into various cell types, making them ideal candidates for regenerative therapies.²² In contrast, GFs, which are abundant in the connective tissue surrounding teeth, play an essential role in wound healing and extracellular matrix synthesis, thereby maintaining periodontal tissue integrity.²³ In this study, the regenerative potential of these 2 cell types

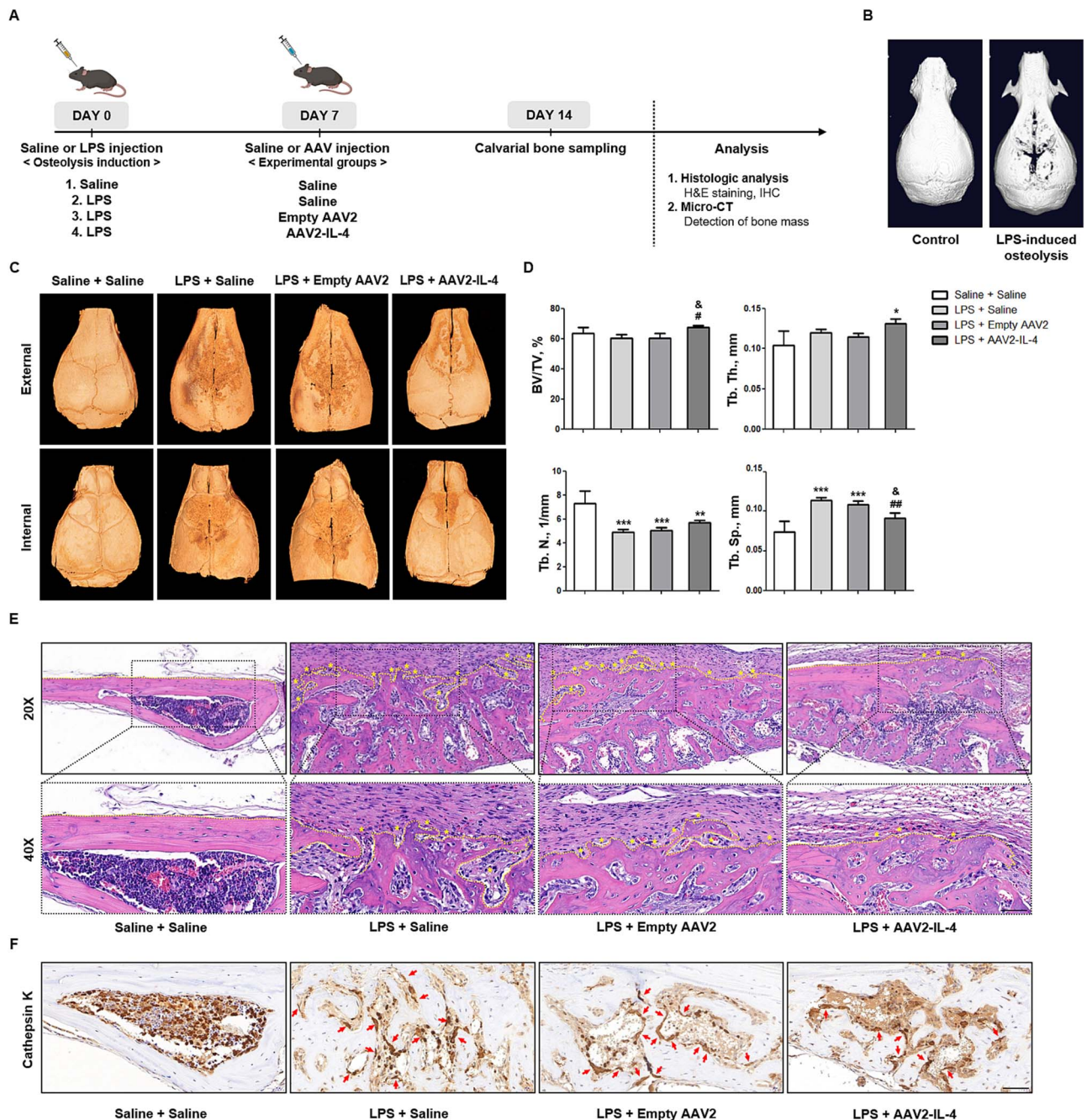


Figure 5. AAV2-IL4 injection promoted bone regeneration in an LPS-induced calvarial osteolysis model. (A) Illustration of the in vivo experimental design. (B) In vivo micro-CT images of the calvarial bone after LPS treatment. (C) Representative micro-CT images of reconstructed mouse calvaria from each group. (D) Quantification of bone volume fraction (BV/TV), trabecular number (Tb.N.), trabecular separation (Tb.Sp.), and trabecular thickness (Tb.Th.). Representative images of calvarial bone sections stained with hematoxylin and eosin (H&E) (E) and immunohistochemical staining for cathepsin K (F). Scale bar = 50 μ m. Compared with the saline + saline group: * $p < .05$, ** $p < .01$, *** $p < .001$. Compared with the LPS + saline group: # $p < .05$, ## $p < .01$. Compared with the LPS + empty AAV2 group: & $p < .05$. $N = 4$. Abbreviations: AAV, adeno-associated virus; LPS, lipopolysaccharide.

was explored by assessing the transduction efficiency of AAV serotypes in both rat and human DPSCs and GFs.

The controlled or sustained delivery of growth factors, cytokines, and chemokines that promote osteogenic differentiation is crucial for bone regeneration.²⁴ Protein-based therapies offer a direct means of supplementing deficient proteins but have a short half-life, poor stability, and low solubility, so it requires frequent, high-dose administrations.²⁵ In contrast, local gene therapy can overcome these limitations by enabling prolonged and localized protein expression.

Among viral vectors, AAV is particularly attractive for gene therapy applications due to its ability to persist as an episome rather than integrating into the host genome, thereby minimizing the risk of insertional mutagenesis while exhibiting low immunogenicity.²⁶ However, the tropism and transduction efficiency of AAV vectors vary among serotypes, influencing their efficacy for specific target tissues.²⁷ AAV2, the first identified serotype, has been extensively studied and displays broad tropism across various tissues.²⁸ AAV1 efficiently transduces the respiratory tract, muscle, central

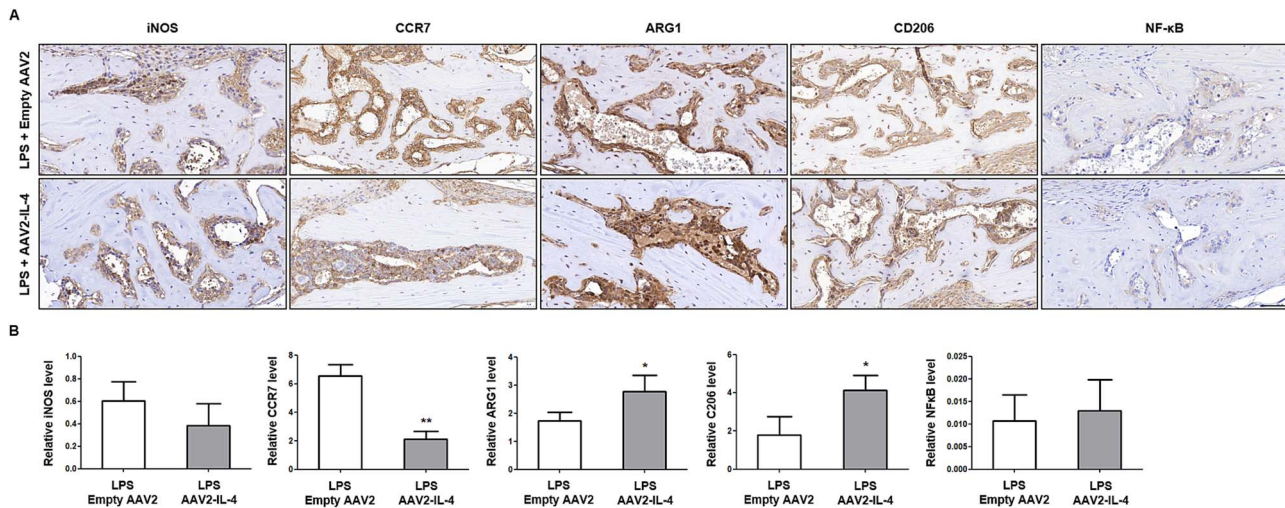


Figure 6. Immunohistochemical analysis of macrophage polarization in calvarial sections. (A) Representative immunohistochemical staining images of iNOS, CCR7, ARG1, CD206, and NF- κ B in calvarial bone sections. (B) Quantification of positive staining for iNOS, CCR7, ARG1, CD206, and NF- κ B. Scale bar = 50 μ m. * p < .05. ** p < .01. N = 4.

nervous system (CNS), and retina; AAV5 targets the CNS, liver, and retina; and AAV6 is particularly effective in the heart, muscle, and liver.²⁸ Additionally, AAV1, AAV2, and AAV6 have shown good transduction capabilities in many stem cells.²⁸

In this study, we assessed the transduction efficiency of 4 AAV serotypes by quantifying the proportion of ZsGreen1⁺ cells following transduction with AAV1-, AAV2-, AAV5-, and AAV6-ZsGreen1 in rGFs, rDPSCs, hGFs, and hDPSCs. All serotypes successfully delivered the ZsGreen1 gene to these cell types; however, AAV2, followed by AAV6, exhibited the highest transduction efficiency. Notably, AAV5 was more effective than AAV1 in rat cells, whereas the reverse was observed in human cells. AAV2 has been reported to strongly interact with heparin sulfate proteoglycans (HSPGs) on the cell surface, which serve as primary attachment receptors facilitating viral entry.²⁹ HSPGs are highly abundant in vascularized tissues,³⁰ including dental pulp,³¹ which may contribute to the high transduction efficiency of AAV2 in DPSCs. To our knowledge, this is the first report to compare AAV serotype transduction efficiency in both rat and human GFs and DPSCs.

We also established IL-4-overexpressing rDPSCs and hDPSCs using AAV vectors to investigate their osteogenic differentiation potential. AAV-mediated IL-4 overexpression significantly upregulated osteogenic differentiation markers and enhanced calcium deposition. IL-4, an anti-inflammatory cytokine, plays a pivotal role in type II inflammatory responses and tissue regeneration.³² Previous studies suggest that IL-4 promotes bone formation by inhibiting osteoclast differentiation while stimulating ALP activity in osteoblast-like cells.¹⁰ Additionally, the inactivation of IL-4 and IL-13 has been associated with reduced cortical bone mass in adult male mice.³³ Moreover, IL-4-overexpressing MSCs engineered via lentiviral vectors have been shown to enhance osteogenesis and promote M2 macrophage polarization in a long bone defect model.³⁴ IL-4 has also been implicated in promoting pancreatic cancer cell proliferation and regulating Th2-cell differentiation via the ERK signaling pathway.^{35,36} The ERK signaling pathway, one of the MAPK pathways,

regulates fundamental cellular processes such as proliferation, differentiation, and apoptosis.³⁷ Among the MAPK family members, including p38, JNK, and ERK, ERK has been identified as a crucial regulator of osteogenic differentiation.³⁸ Several studies have demonstrated that ERK activation facilitates osteoblast differentiation and skeletal mineralization.^{39,40}

This study suggests a bone regeneration strategy that can produce dual effects, ie, immunomodulation and osteogenic differentiation, through IL-4 gene delivery using AAVs. Recent studies in osteoimmunology have shown that immune microenvironments significantly contribute to bone tissue formation.^{41,42} Depending on the microenvironment, macrophages can polarize into M1 macrophages by interferon- γ , which promote inflammation, or M2 macrophages by IL-4, which regulate tissue repair processes.⁴³ The transition from M1 to M2 macrophages is a pivotal process in ensuring optimal bone regeneration.⁴⁴ Therapies targeting macrophage polarization, whether by directly modulating macrophage phenotypes or delivering regulatory cytokines, have demonstrated potential in enhancing bone regeneration.^{45,46} While most current approaches in bone regeneration modulating macrophages have focused on promoting an abundant M2 macrophage phenotype,⁴⁷⁻⁴⁹ excessive M2 macrophage activation may lead to fibrosis.⁵⁰ By leveraging AAV-mediated IL-4 gene delivery, we sought to achieve sustained, low-level IL-4 expression, thereby preventing excessive polarization toward the M2 phenotype while maintaining an environment conducive to bone regeneration. In this study, AAV2-IL-4 injection created a favorable microenvironment for in vivo bone regeneration by synergistically promoting direct osteoinduction and M2 macrophage activation.

In conclusion, among the 4 AAV serotypes examined, AAV2 exhibited the highest gene-transfer efficiency in dental mesenchymal cells and demonstrated the most prolonged IL-4 expression. IL-4 overexpression activated the ERK pathway and promoted the osteogenic differentiation of both rat and human DPSCs. Moreover, in the calvarial osteolysis model, AAV2-mediated IL-4 delivery facilitated M2 macrophage polarization and promoted bone regeneration, effectively

mitigating bone loss. This study highlights the potential of AAV2-mediated IL-4 gene delivery as a novel therapeutic strategy for periodontal bone regeneration, suggesting its utility in bone regeneration therapies. Further studies should be pursued to understand the mechanisms controlling macrophage polarization, particularly in the context of the bone microenvironment, to develop new strategies for improving outcomes in bone regenerative therapies.

Author contributions

Hyewon Kim (Conceptualization, Data curation, Formal analysis, Investigation, Methodology, Project administration, Validation, Visualization, Writing—original draft, Writing—review & editing, Supervision), Kyoung-Hwa Kim (Conceptualization, Investigation, Methodology), Leewoo Kang (Investigation, Methodology), Yang-Jo Seol (Validation, Writing—review & editing), Shin Hye Chung (Project administration, Validation, Writing—review & editing), and Shin-Young Park (Project administration, Validation, Supervision, Writing—review & editing).

Supplementary material

Supplementary material is available at *JBMR Plus* online.

Funding

This research was supported by the Basic Science Research Program through the National Research Foundation of Korea funded by the Ministry of Education [grant nos. 2022R1A2C1012354, 2022R1A6A3A01086548, and 2021R1A6A1A03039462].

Conflicts of interest

The authors declare that there is no conflict of interest regarding the publication of this article.

Data availability

The data used to support the finding of this study are available from the corresponding author upon request.

References

- Kinane DF, Stathopoulou PG, Papapanou PN. Periodontal diseases. *Nat Rev Dis Primers*. 2017;3(1). <https://doi.org/10.1038/nrdp.2017.38>
- Kornman KS. Mapping the pathogenesis of periodontitis: a new look. *J Periodontol*. 2008;79(8S):1560–1568. <https://doi.org/10.1902/jop.2008.080213>
- Bartold PM, Van Dyke TE. Host modulation: controlling the inflammation to control the infection. *Periodontol*. 2017;75(1):317–329. <https://doi.org/10.1111/prd.12169>
- Yao Y, Cai X, Ren F, et al. The macrophage-osteoclast axis in osteoimmunity and osteo-related diseases. *Front Immunol*. 2021;12. <https://doi.org/10.3389/fimmu.2021.664871>
- Cekici A, Kantarci A, Hasturk H, Van Dyke TE. Inflammatory and immune pathways in the pathogenesis of periodontal disease. *Periodontol*. 2014;64(1):57–80. <https://doi.org/10.1111/prd.12002>
- Madeira MF, Queiroz-Junior CM, Costa GM, et al. MIF induces osteoclast differentiation and contributes to progression of periodontal disease in mice. *Microbes Infect*. 2012;14(2):198–206. <https://doi.org/10.1016/j.micinf.2011.09.005>
- Van Dyke TE, Sima C. Understanding resolution of inflammation in periodontal diseases: is chronic inflammatory periodontitis a

- failure to resolve? *Periodontol*. 2020;82(1):205–213. <https://doi.org/10.1111/prd.12317>
- Zhang S, Chuah SJ, Lai RC, Hui JHP, Lim SK, Toh WS. MSC exosomes mediate cartilage repair by enhancing proliferation, attenuating apoptosis and modulating immune reactivity. *Biomaterials*. 2018;156:16–27. <https://doi.org/10.1016/j.biomaterials.2017.11.028>
 - Li D, Li X, Zhang J, Tang Z, Tian A. The immunomodulatory effect of IL-4 accelerates bone substitute material-mediated osteogenesis in aged rats via nlrp3 inflammasome inhibition. *Front Immunol*. 2023;14:1121549. <https://doi.org/10.3389/fimmu.2023.1121549>
 - Yamada A, Takami M, Kawawa T, et al. Interleukin-4 inhibition of osteoclast differentiation is stronger than that of interleukin-13 and they are equivalent for induction of osteoprotegerin production from osteoblasts. *Immunology*. 2007;120(4):573–579. <https://doi.org/10.1111/j.1365-2567.2006.02538.x>
 - Watanabe K, Tanaka Y, Morimoto I, et al. Interleukin-4 as a potent inhibitor of bone resorption. *Biochem Biophys Res Commun*. 1990;172(3):1035–1041. [https://doi.org/10.1016/0006-291X\(90\)91550-C](https://doi.org/10.1016/0006-291X(90)91550-C)
 - Sato T, Pajarinen J, Behn A, et al. The effect of local IL-4 delivery or ccl2 blockade on implant fixation and bone structural properties in a mouse model of wear particle induced osteolysis. *J Biomed Mater Res A*. 2016;104(9):2255–2262. <https://doi.org/10.1002/jbm.a.35759>
 - Favier AL, Nikovics K. Molecular and cellular mechanisms of inflammation and tissue regeneration. *Biomedicines*. 2023;11(5):1416. <https://doi.org/10.3390/biomedicines11051416>
 - Kimelman Bleich N, Kallai I, Lieberman JR, Schwarz EM, Pelled G, Gazit D. Gene therapy approaches to regenerating bone. *Adv Drug Deliv Rev*. 2012;64(12):1320–1330. <https://doi.org/10.1016/j.addr.2012.03.007>
 - Maurya S, Sarangi P, Jayandharan GR. Safety of adeno-associated virus-based vector-mediated gene therapy-impact of vector dose. *Cancer Gene Ther*. 2022;29(10):1305–1306. <https://doi.org/10.1038/s41417-021-00413-6>
 - Park SY, Kim KH, Kim S, Lee YM, Seol YJ. BMP-2 gene delivery-based bone regeneration in dentistry. *Pharmaceutics*. 2019;11(8):393. <https://doi.org/10.3390/pharmaceutics11080393>
 - Liu Y, Xiong W, Li J, et al. Application of dental pulp stem cells for bone regeneration. *Front Med (Lausanne)*. 2024;11. <https://doi.org/10.3389/fmed.2024.1339573>
 - Bertassoli BM, Costa ES, Sousa CA, et al. Rat dental pulp stem cells: isolation and phenotypic characterization method aiming bone tissue bioengineering. *Braz Arch Biol Technol*. 2016;59. <https://doi.org/10.1590/1678-4324-2016150613>
 - Sonoda S, Mei YF, Atsuta I, et al. Exogenous nitric oxide stimulates the odontogenic differentiation of rat dental pulp stem cells. *Sci Rep*. 2018;8(1):3419. <https://doi.org/10.1038/s41598-018-21183-6>
 - Long W, Quan J, Liu Y, Li J, Gong Q, Jiang H. 7nd protein exerts inhibitory effects on both osteoclast differentiation in vitro and lipopolysaccharide-induced bone erosion in vivo. *Mol Med Rep*. 2020;22(1):97–104. <https://doi.org/10.3892/mmr.2020.11119>
 - Yamada Y, Ito K, Nakamura S, Ueda M, Nagasaka T. Promising cell-based therapy for bone regeneration using stem cells from deciduous teeth, dental pulp, and bone marrow. *Cell Transplant*. 2011;20(7):1003–1013. <https://doi.org/10.3727/096368910X539128>
 - Tatullo M, Marrelli M, Shakesheff KM, White LJ. Dental pulp stem cells: function, isolation and applications in regenerative medicine. *J Tissue Eng Regen Med*. 2015;9(11):1205–1216. <https://doi.org/10.1002/term.1899>
 - Haniffa MA, Collin MP, Buckley CD, Dazzi F. Mesenchymal stem cells: the fibroblasts' new clothes? *Haematologica*. 2009;94(2):258–263. <https://doi.org/10.3324/haematol.13699>
 - Dimitriou R, Jones E, McGonagle D, Giannoudis PV. Bone regeneration: current concepts and future directions. *BMC Med*. 2011;9(1). <https://doi.org/10.1186/1741-7015-9-66>

25. Leader B, Baca QJ, Golan DE. Protein therapeutics: a summary and pharmacological classification. *Nat Rev Drug Discov.* 2008;7(1): 21–39. <https://doi.org/10.1038/nrd2399>
26. Wang D, Tai PWL, Gao G. Adeno-associated virus vector as a platform for gene therapy delivery. *Nat Rev Drug Discov.* 2019;18(5): 358–378. <https://doi.org/10.1038/s41573-019-0012-9>
27. Issa SS, Shaimardanova AA, Solovyeva VV, Rizvanov AA. Various AAV serotypes and their applications in gene therapy: an overview. *Cells.* 2023;12(5):785–826. <https://doi.org/10.3390/cells12050785>
28. Ellis BL, Hirsch ML, Barker JC, Connelly JP, Steininger RJ 3rd, Porteus MH. A survey of ex vivo/in vitro transduction efficiency of mammalian primary cells and cell lines with nine natural adeno-associated virus (AAV1-9) and one engineered adeno-associated virus serotype. *Virology.* 2013;10(1):74. <https://doi.org/10.1186/1743-422X-10-74>
29. Negishi A, Chen J, McCarty DM, Samulski RJ, Liu J, Superfine R. Analysis of the interaction between adeno-associated virus and heparan sulfate using atomic force microscopy. *Glycobiology.* 2004;14(11):969–977. <https://doi.org/10.1093/glycob/cwh118>
30. Pretorius D, Richter RP, Anand T, Cardenas JC, Richter JR. Alterations in heparan sulfate proteoglycan synthesis and sulfation and the impact on vascular endothelial function. *Matrix Biol Plus.* 2022;16:100121. <https://doi.org/10.1016/j.mbplus.2022.100121>
31. Hayano S, Kurosaka H, Yanagita T, et al. Roles of heparan sulfate sulfation in dentinogenesis. *J Biol Chem.* 2012;287(15): 12217–12229. <https://doi.org/10.1074/jbc.M111.332924>
32. Junttila IS. Tuning the cytokine responses: an update on interleukin (IL)-4 and IL-13 receptor complexes. *Front Immunol.* 2018;9:888. <https://doi.org/10.3389/fimmu.2018.00888>
33. Silfverswärd CJ, Larsson S, Ohlsson C, Frost A, Nilsson O. Reduced cortical bone mass in mice with inactivation of interleukin-4 and interleukin-13. *J Orthop Res.* 2007;25(6): 725–731. <https://doi.org/10.1002/jor.20361>
34. Ueno M, Lo CW, Barati D, et al. Interleukin-4 overexpressing mesenchymal stem cells within gelatin-based microribbon hydrogels enhance bone healing in a murine long bone critical-size defect model. *J Biomed Mater Res A.* 2020;108(11):2240–2250. <https://doi.org/10.1002/jbm.a.36982>
35. Tripathi P, Sahoo N, Ullah U, et al. A novel mechanism for ERK-dependent regulation of il4 transcription during human th2-cell differentiation. *Immunol Cell Biol.* 2012;90(7):676–687. <https://doi.org/10.1038/icb.2011.87>
36. Prokopchuk O, Liu Y, Henne-Bruns D, Kornmann M. Interleukin-4 enhances proliferation of human pancreatic cancer cells: evidence for autocrine and paracrine actions. *Br J Cancer.* 2005;92(5): 921–928. <https://doi.org/10.1038/sj.bjc.6602416>
37. Guo YJ, Pan WW, Liu SB, Shen ZF, Xu Y, Hu LL. ERK/MAPK signalling pathway and tumorigenesis. *Exp Ther Med.* 2020;19(3): 1997–2007. <https://doi.org/10.3892/etm.2020.8454>
38. Schindeler A, Little DG. Ras-MAPK signaling in osteogenic differentiation: friend or foe? *J Bone Miner Res.* 2006;21(9):1331–1338. <https://doi.org/10.1359/jbmr.060603>
39. Salaszyk RM, Klees RF, Hughlock MK, Plopper GE. ERK signaling pathways regulate the osteogenic differentiation of human mesenchymal stem cells on collagen I and vitronectin. *Cell Commun Adhes.* 2004;11(5–6):137–153. <https://doi.org/10.1080/15419060500242836>
40. Xiao G, Jiang D, Thomas P, et al. Mapk pathways activate and phosphorylate the osteoblast-specific transcription factor, cbfa1. *J Biol Chem.* 2000;275(6):4453–4459. <https://doi.org/10.1074/jbc.275.6.4453>
41. Niu Y, Wang Z, Shi Y, Dong L, Wang C. Modulating macrophage activities to promote endogenous bone regeneration: biological mechanisms and engineering approaches. *Bioact Mater.* 2021;6(1): 244–261. <https://doi.org/10.1016/j.bioactmat.2020.08.012>
42. Xie Y, Hu C, Feng Y, et al. Osteoimmunomodulatory effects of biomaterial modification strategies on macrophage polarization and bone regeneration. *Regen Biomater.* 2020;7(3):233–245. <https://doi.org/10.1093/rb/rbaa006>
43. Oishi Y, Manabe I. Macrophages in inflammation, repair and regeneration. *Int Immunol.* 2018;30(11):511–528. <https://doi.org/10.1093/intimm/dxy054>
44. Gou M, Wang H, Xie H, Song H. Macrophages in guided bone regeneration: potential roles and future directions. *Front Immunol.* 2024;15:1396759. <https://doi.org/10.3389/fimmu.2024.1396759>
45. Huang R, Wang X, Zhou Y, Xiao Y. Rankl-induced m1 macrophages are involved in bone formation. *Bone Res.* 2017; 5(1):17019. <https://doi.org/10.1038/boneres.2017.19>
46. Sonomoto K, Yamaoka K, Oshita K, et al. Interleukin-1 β induces differentiation of human mesenchymal stem cells into osteoblasts via the wnt-5a/receptor tyrosine kinase-like orphan receptor 2 pathway. *Arthritis Rheum.* 2012;64(10):3355–3363. <https://doi.org/10.1002/art.34555>
47. Fan S, Zhang C, Sun X, et al. Metformin enhances osteogenic differentiation of bmsc by modulating macrophage m2 polarization. *Sci Rep.* 2024;14(1):20267. <https://doi.org/10.1038/s41598-024-71318-1>
48. Chen W, Ma L, Sun W, et al. Cgrp promotes osteogenic differentiation by regulating macrophage m2 polarization through hdac6/akap12 signaling pathway. *Regen Med.* 2024;19(7–8): 379–391. <https://doi.org/10.1080/17460751.2024.2370697>
49. Cai G, Lu Y, Zhong W, et al. Piezo1-mediated m2 macrophage mechanotransduction enhances bone formation through secretion and activation of transforming growth factor- β 1. *Cell Prolif.* 2023;56(9):e13440. <https://doi.org/10.1111/cpr.13440>
50. Braga TT, Agudelo JS, Camara NO. Macrophages during the fibrotic process: M2 as friend and foe. *Front Immunol.* 2015;6:602–617. <https://doi.org/10.3389/fimmu.2015.00602>